A Study on a New Synthetic Method of CdS, CdSe, CdTe and ZnS Nanomaterials by γ-Irradiation

γ선으로 CdS, CdSe, CdTe 그리고 ZnS의 나노물질의 새로운 합성방법에 관한 연구

Advisor : Young-Soo Kang

A thesis submitted in partial fulfillment of the requirements. for the degree of

Master of Science

in the Departement of Chemistry, Graduate School, Pukyong National University

August 2004

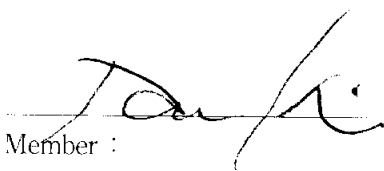# A Study on New Synthetic Method of CdS, CdSe, CdTe and ZnS Nanomaterials by γ-Irradiation

A Dissertation

by

Song-Ja Jo

Approved as to style and content by :

Chair man :

Member :   Member :

June 24. 2004

Contents

List of Figures

Figure   9   Transmission electron microscopy (TEM) images of CdS nanoparticles synthesized by γ-irradiation as the change of absorbed dose of (a) 24,000 Gy, (b) 70,000 Gy, and (c) 90,000 Gy.

Figure   10   Diagram on the size distribution of CdS nanoparticles synthesized by γ-irradiation as the change of absorbed doses (a) no irradiation (b) 24,000 Gy, (c) 70,000 Gy, and (d) 90,000 Gy.

Figure   11   Transmission electron microscopy (TEM) images of CdS nanoparticles synthesized by γ-irradiation as the change of the concentration of oleate as a surfactant; Molar ratio between reactants as (a) Cd^{2+} : oleate = 1 : 2 (a standard) and (b) Cd^{2+} : oleate = 1 : 4.

Figure   12   Transmission electron microscopy (TEM) images of CdSe nanoparticles synthesized by γ-irradiation as the change of absorbed doses of (a) 30,000 Gy, (b) 70,000 Gy, and (c) 90,000 Gy.

Figure   13   Transmission electron microscopy (TEM) image of CdTe nanoparticles synthesized by γ-irradiation with a dose of 90,000 Gy.

Figure   14   Transmission electron microscopy (TEM) images of ZnS nanoparticles synthesized by γ-irradiation as the change of absorbed doses of (a) 30,000 Gy, (b) 50,000 Gy, (c) 70,000 Gy, and (d) 90,000 Gy.

List of Tables

A Study on a New Synthetic Method of CdS, CdSe, CdTe and ZnS
Nanomaterials by γ-Irradiation

Song-Ja Jo

Department of Chemistry, Graduate School
Pukyong National University

Abstract

Semiconducting materials (CdS, CdSe, CdTe, and ZnS) were synthesized by a new method of γ-irradiation. The method using γ-irradiation was done in the mild condition at room temperature and the atmospheric pressure. The synthesis was done using oleate as a surfactant. The synthesis of nanorods and nanowires was carried out using ethylendiamine (ed) and pyridine (py) as solvents. Their structure was determined with X-ray powder diffraction (XRD) and X-ray photoelectron spectroscopy (XPS). Energy dispersive X-ray spectrometer (EDX) was used to characterize the elements. Transmission electron microscopy (TEM) was used to determine the size and the morphology of them. The optical properties of the products were studied with UV-visible absorption spectra.

1. Introduction

The special properties of nanomaterials have attracted much interest.[1-3,62-63] There is a great deal of interest in finding new synthetic routes to prepare nanomaterials. With crystal size decreasing, the energy band of semiconductor nanocrystallites evolves from sequential to discrete energy levels, which causes semiconductor nanocrystallites to display optical, electronic and structural properties to be different from those of bulk phase and isolated atoms.[4-19] Altering the size of the particles affects the degree of the confinement of the electrons and changes the electronic structures of the solid, especially the band gap edges, which are tunable with particle size. Among a variety of semiconducting materials, the binary metal chalcogenides of group II have been extensively studied. Several methods have been developed to synthesize this kind of nanoparticles, for instance, preparing in microemulsions,[14-15] in vesicles,[13] or from precursors.[12] More recently CdS, CdSe, and CdTe particles capped with tri-n-octylphosphine/tri-n-octylphosphine oxide (TOP/TOPO) have been prepared by reacting organometallic reagents in the coordinating solvents at 300 ℃.[12,23,26,32]

Also unique structure, optical and electrical properties of one-dimensional (1D) semiconductors and metals make them be the key structural blocks for a new generation electronics, sensors, and photonics materials.[36-49] Several synthetic methods of nanorod and nanowire production have been developed, but they all are based on point-initiated uniaxial growth of the crystal. The methods of nanorods and nanowires were been prepared previously using several approaches including laser-assisted catalytic[41] and vapor-phase growth method,[42,44,46] electrochemical method,[40] and using template (as DNA,[49] cytochrome[39]), block copolymer (as double-hydrophilic block copolymer[45]).

To prepare metal chalcogenides nanoparticles, the reaction sources used are usually toxic H_2S,[21,22] CS_2,[25] and the noxious surfactants as TOP/TOPO.[12,23,26,32]

These methods are prepared at above high pressure[29,36] or below low pressure to the extent of ~ 1 torr[12] at high temperature above 500 ℃.[42,44,46] In case of nanorods and nanowires, the heterogeneous reactants also produced by laser ablation and difficulty in controlling nucleation in vapor-phase growth have limited the control of key properties with these methods. Another method need the various templates and they should be removed from the synthesized materials after finished the synthetic reaction.

A γ-irradiation method has been applied to prepare many ultrafine metal and oxide powders.[50-61] Qian's group synthesized nanocrystalline indium, PbS, CuS and analyzed their properties.[50-52] In general, the γ-irradiation method performed without toxic H_2S, CS_2, and TOP/TOPO, is a mild way to synthesize nanometer materials at the ambient conditions without high temperature and pressure. Due to the work at the atmospheric pressure and room temperature, this method can be used as a new method for the synthesis of inorganic nanoparticles via more simple process than one used in the past. When it is done by γ-irradiation, the solution system maintains a reducing atmosphere which reduces high valent metal ions to low valency. In this paper, we report a novel and easy-to-manipulate method to prepare the ordered semiconducting materials by γ-irradiation.

2. Experiment

2-1. Materials

All chemicals used were of analytical grade or of the highest purity available. Cadmium chloride hemipentahydrate (CdCl$_2$ · 5/2H$_2$O, 99%), selenium (Se, 200 mesh 99.5+%) and tellurium (Te, 99.8%) were obtained from Aldrich Chemical Company Inc. Sodium sulfide nonahydrate (Na$_2$S · 9H$_2$O, 98+%) was obtained from Across Organics. Zinc chloride (ZnCl$_2$, 96%), sodium oleate (C$_{17}$H$_{33}$COONa, 98%) and ethylenediamine (ed) were obtained from Junsei Chemical Company Co., Ltd. Sodium borohydride (NaBH$_4$, 98%) was obtained from Sigma Chemical Company Inc. Pyridine (py) was from Kanto Chemical Company Inc. All reagent-grade chemicals were used as received, and house-distilled water was passed through a four-cartridge Barnstead Nanopure II purification train consisting of Macropure pretreatment, organic free, and a 0.2 μm hollow-fiber final filter for removing particles. Its resistivity was determined as 18.4 MΩ and used throughout.

2-2. Methods

2-2-1. Preparation of NaHSe and NaHTe

Using a 2 : 1 molar ratio of borohydride to selenium in water, the reaction proceeded with hydrogen evolution to from sodium hydrogen selenide. Briefly, sodium borohydride (2 mmol) was transferred to a small flask, then 1 mL ultrapure water was added, after which selenium powder (1 mmol) was added to the flask. The flask was sealed quickly with a small pinhole exposed to atmosphere and was placed on ice. A rapid reaction evolved hydrogen gas in

the flask. Approximately 30 min later, the black selenium powder disappeared completely and white crystals appeared in the bottom of the flask. The resulting clear aqueous solution was then transferred carefully, using a syringe, into 100 mL of degassed water in a volumetric flask sealed with a rubber plug. The NaHSe[33] solution was freshly prepared prior to each nanocolloid preparation and kept for no longer than 3 days. NaHTe[31] was synthesized with the same method such as NaHSe.

2-2-2. Preparation of CdS, CdSe, CdTe and ZnS nanoparticles

Sodium oleate (10 mmol) was dissolved in 80 mL of water to obtain aqueous solution. $CdCl_2 \cdot 5/2H_2O$ (5 mmol) was dissolved in 1 mL of water and mixed with the prepared sodium oleate solution. $Na_2S \cdot 9H_2O$ (5 mmol) powders were added into mixed solution of sodium oleate and $CdCl_2$ and then continuously stirred for 2 hrs. Then, the reactant solution was irradiated by γ-irradiation for a given absorbed dose in the field of a ^{60}Co γ-ray source. The synthesis of semiconducting materials was done by changing the dose of γ-irradiation. The product was washed with acetone, filtered and then dried at the room temperature. CdSe, CdTe and ZnS particles were synthesized with the same method.

2-2-3. Preparation of CdS, CdSe, CdTe, ZnS and ZnSe nanorods and nanowires

Sodium oleate (10 mmol) was dissolved in 40 mL of pure water. Cadmium chloride hemipentahydrate (5 mmol) was dissolved in 1 mL of water and mixed with the prepared sodium oleate solution and stirred for 2 hrs. The mixture was filtered and dried at room temperature.

Cadmium oleate mixture (5 mmol) was dissolved in 40 mL of

ethylendiamine. $Na_2S \cdot 9H_2O$ (5 mmol) was added into the dissolved solution of cadmium oleate and then stirred for 2 hrs. The reactants were irradiated by γ-irradiation in the field of a ^{60}Co γ-ray source. The product was washed with absolute ethanol, diluted HCl solution (0.1 M) and absolute ethanol, filtered and then dried at room temperature. In case of nanowires, the solvent was changed from ethylendiamine to pyridine. Nanorods and nanowires of CdSe, CdTe, ZnS and ZnSe were synthesized with the same method.

2-3. Apparatus

The samples were characterized by X-ray powder diffraction (XRD) patterns to investigate the crystal structure. X-ray powder diffraction (XRD) spectra were collected using a Philips, X'Pert-MPD system. Transmission electron microscopy (TEM) was used to study on the morphology and particle sizes. Transmission electron microscopy (TEM) image was obtained using a Hitachi model S-2400. Samples for TEM were prepared on 300 mesh copper grids coated with carbon. A drop of material solutions was carefully placed on the copper grid surface and dried. Electron diffraction (ED) patterns and high resolution transmission electron microscopy (HR-TEM) images were obtained using a Jeol model JEM-2010. Energy dispersive X-ray (EDX) spectra were obtained using a HITACHI model, H-7500. The X-ray photoelectron spectroscopy (XPS) study was performed with a VG-Scientific ESCALAB 250 spectrometer with monocromatized Al Kα X-ray source at Korea Basic Science Institute. The UV-visible absorption spectra were obtained to study on the optical properties of the synthesized CdS nanoparticles. The UV-visible absorption spectrum was recorded on a Varian Carry. The photoluminescence (PL) spectra were obtained to study on the optical properties of the synthesized CdS nanoparticles. Photoluminescence spectra were recorded on a Perkin-Elmer (LS50B).

3. Background

3-1. Nanoparticles

Nanoparticles are generally considered to be a number of atoms or molecules bonded together with a radius of < 100 nm.[62-63] A nanometer is 10^{-9} m or 10 Å, so particles having a radius of about ≤ 1,000 Å can be considered to be nanoparticles. This definition based on size is not totally satisfactory because it does not really distinguish between molecules and nanoparticles. They can be built by assembling individual atoms or subdividing bulk materials. What makes nanoparticles very interesting and endows them with their unique properties is that their size is smaller than critical lengths that characterize many physical phenomena, electronic properties, optical properties.[1-38]
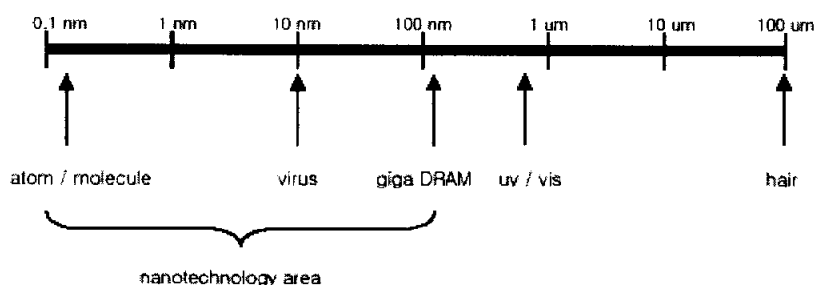
Figure 1   Scale measure for nanotechnology.

Many synthetic methods for the preparation of nano-dispersed material have been reported; several routes involve colloidal chemistry, with others involving the kinetically controlled precipitation of nanocrystallites, using organometallic compounds.[4-11] Controlled precipitation reactions can yield dilute suspensions of quasi monodispersed particles. This synthetic method sometimes involves the

use of seeds of very small particles for the subsequent growth of larger ones.[13] Brus et al.[15] prepared CdS nanoparticles which involves the controlled nucleation of CdS on mixing of dilute aqueous solutions of $CdSO_4$ and $(NH_4)_2S$. Silylorganochalcogenides reacted readily with metal salts or simple metal alkyls to form metal-chalcogenide bonds.[14-15] Micelle stabilized CdSe nanocrystallites, with Cd^{2+} rich surfaces, react similarly with $R[(CH_3)_3Si]_2Se$ to give larger CdSe crystallites encapsulated by a layer of organic ligands (R) These surface passivated crystallites can be isolated as powders, which are soluble in organic solvents such as pyridine. A powerful method for the preparation of semiconductor nanocrystallites has been described by Murray, Norris, and Bawendi;[12] solutions of $(CH_3)_2Cd$ and tri-n-octylphosphine selenide (TOPSe) are injected into hot tri-n-octylphosphine oxide (TOPO) in the temperature range of 120 - 300 ℃. This produced TOPO capped nanocrystallites of CdSe. The use of single source precursors in the deposition of thin film compound semiconductors by MOCVD techniques has been extensively studied.[16-18] Related compounds can be used to prepare compound semiconductor nanoparticles, such as oligomeric $Cd(Se(C_2H_5))_2$ or metal dithiocarbamates in 4-ethylpyridine.[19]

One of the major goals in research on nanocrystallites is to make use of their unique properties in novel electronic devices.[1-3,62-63] The production of any such devices will require the assembly and manipulation of semiconductor nanoparticles without loss of their unique properties. Two fundamental factors, both related to the size of the individual nanocrystal, distinguish their behavior from the corresponding macrocrystalline material. At first, the transition of semiconductors occurs for a given temperature at a relatively large size compared to metals, insulators, or molecular crystals. This difference can be understood by considering that the bands of a solid are centered about atomic energy levels, with the width of the band related to the strength of the nearest-neighbor interactions. The Fermi level lies between two bands, such that the edges of the bands dominate the low-energy optical and electrical behavior. Optical excitations across the gap depend strongly on size for clusters as large as 10,000 atoms. Electrical transport also depends strongly on size, mainly because of the large variation in energy required to add or

remove charges on a nanocrystal. A second important characteristic of semiconductors concerns the influence of the surface on optical and electrical properties, and the need to embed semiconductor clusters in a passivating medium. At the surface of a pure inorganic semiconductor, substantial reconstructions in the atomic position occur, invariably leading to energy levels within the energetically forbidden gap of the bulk solid. These surface states trap electrons or holes and degrade the electrical and optical properties of the material. Passivation is the chemical process by which these surface atoms are bonded to another material of a much larger band gap, eliminating all of the energy levels inside of the gap. The ideal termination naturally removes the structural reconstructions, leaving no strain, and simply produces an atomically abrupt jump in the chemical potential for electrons or holes at the interface. This potential confines electrons or holes inside the cluster, much like the "particle in a box" of elementary quantum mechanics.
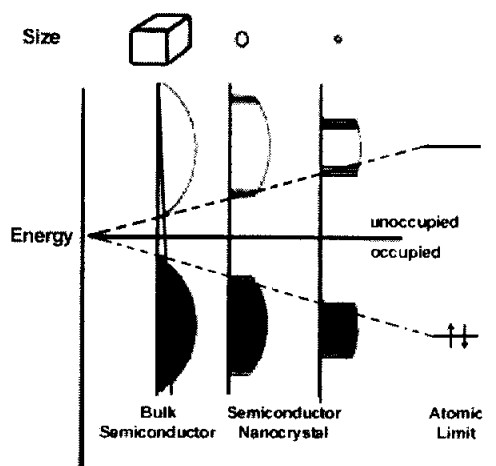
Figure 2   Scheme of the density of states in semiconductor clusters.[1,62-63]

3-2. γ -rays

Radioactivity,[64-65] spontaneous disintegration of atomic nuclei by the emission of subatomic particles are called α and β particles, or of electromagnetic rays are called X-rays and γ -rays. This method is done using γ -rays that possess no charge or mass. The emission of γ -rays by a nucleus does not result in a change in chemical properties of the nucleus but merely in the loss of a certain amount of radiant energy. Thus, γ -rays cannot cause such ionization directly, but when they interact with matter they cause the ejection of electrons from atoms. In an interaction due to γ -rays, all or part of the photon energy is transferred to more electrons in the absorber molecule. The produced secondary electrons are energetic and charged. The major types of interaction are photoelectric effect, Compton scattering and pair production. The first process is the photoelectric effect. In this process, the incident X-ray or γ -ray photon interacts with an atom of the absorbing material, and the photon completely disappears. Its energy is transferred to one of the orbital electrons of the atom. Because this energy in general far exceeds the binding energy of the electron in the host atom, the electron is ejected at high velocity. The kinetic energy of this secondary electron is equal to the incoming energy of the photon minus the binding energy of the electron in the original atomic shell. The process leaves the atom with a vacancy in one of the normally filled electron shells, which is then refilled after a short period of time by a nearby free electron. This filling process again liberates the binding energy in the form of a characteristic X-ray photon, which then typically interacts with electrons from less tightly bound shells in nearby atoms, producing additional fast electrons. The overall effect is therefore the complete conversion of the photon energy into the energy carried by fast electrons. Since the fast electrons are now detectable through their Coulombic interactions, they can serve as the basis to indicate the presence of the original γ -ray or X-ray

photon, and a measurement of their energy is tantamount to measuring the energy of the incoming photon. Because the photoelectric process results in complete conversion of the photon energy to electron energy, it is in some sense an ideal conversion step. The task of measuring the γ-ray energy is then reduced to simply measuring the equivalent energy deposited by the fast electrons. Unfortunately, two other types of γ-ray interactions also take place that complicate this interpretation step.

The second mechanism by which γ-rays lose energy is Compton scattering. An incoming γ-ray photon can interact with a single free electron in the absorber. In this process, the photon abruptly changes direction and transfers a portion of its original energy to the electron from which it was scattered, producing an energetic recoil electron. The fraction of the photon energy that is transferred depends on the scattering angle. When the incoming photon is deflected only slightly, little energy is transferred to the electron. Maximum energy transfer occurs when the incoming photon is backscattered from the electron and its original direction is reversed. Since in general all angles of scattering will occur, the recoil electrons are produced with a continuum of energies ranging from near zero to a maximum represented by the backscattering extreme. This maximum energy can be predicted from the conservation of momentum and energy in the photon-electron interaction and is about 0.25 MeV below the incoming photon energy for high-energy γ-rays. After the interaction, the scattered photon has an energy that has decreased by an amount equal to the energy transferred to the recoil electron. It may subsequently interact again at some other location or simply escape from the detector.

A third γ-ray interaction process is pair production. The incoming photon energy is above 1.02 MeV. In the field of a nucleus of the absorber material, the photon may disappear and be replaced by the formation of an electron-positron pair. The minimum energy required to create this pair of particles is their combined rest-mass energy of 1.02 MeV. Therefore, pair

production cannot occur for incoming photon energies below 1.02 MeV. When the photon energy exceeds this value, the excess energy appears as initial kinetic energy shared by the positron and electron that are formed. The positron is a positively charged particle with the mass of a normal negative electron. It slows down and deposits its energy over an average distance that is nearly the same as that for a negative electron of equivalent energy. Therefore both particles transfer their kinetic energy over a distance of no more than a few millimeters in typical solids. The magnitude of the deposited energy is given by the original photon energy minus 1.02 MeV. When the positron member of the pair reaches the end of its track, it combines with a normal negative electron from the absorber in a process known as annihilation. In this step both particles disappear and are replaced by two annihilation photons, each with an energy of 0.511 MeV. Annihilation photons are similar to γ-rays in their ability to penetrate large distances of matter without interacting. They may undergo Compton or photoelectric interactions elsewhere or may escape from detectors of small size.

Ionizing radiation is measured in various units. The oldest unit, the roentgen (R), denotes the amount of radiation that is required to produce 1 electrostatic unit of charge in 1 cubic centimetre of air under standard conditions of pressure, temperature, and humidity. For expressing the dose of radiation absorbed in living tissue, the principal units are the gray (Gy; 1 Gy = 1 joule of radiation energy absorbed per kilogram of tissue) and the rad (1 rad = 100 ergs per gram of tissue = 0.01 Gy). The sievert (Sv) and the rem make it be possible to normalize doses of different types of radiation in terms of relative biologic effectiveness (RBE), since particulate radiations tend to cause greater injury for a given absorbed dose than do X rays or γ-rays. The dose equivalent of a given type of radiation (in Sv) is the dose of the radiation in Gy multiplied by a quality factor that is based on the RBE of the radiation. Hence, one sievert, defined loosely, is that amount of radiation roughly equivalent in biologic effectiveness to one gray of γ-rays (1 Sv = 100 rem).

Because the sievert and the rem are inconveniently large units for certain applications, the milligray (mGy; 1 mGy = 1/1,000 Gy) and millisievert (mSv; 1 mSv = 1/1,000 Sv) are often substituted. The units employed for measuring the amount of radioactivity contained in a given sample of matter are the becquerel (Bq) and the curie (Ci). One becquerel is that quantity of a radioactive element in which there is one atomic disintegration per second; one curie is that quantity in which there are 3.7×10^{10} atomic disintegrations per second (1 Bq = 2.7×10^{-11} Ci). The dose that will accumulate over a given period (say, 50 years) from exposure to a given source of radiation is called the committed dose, or dose commitment.

		The principal units	The oldest units	Conversion factor
	Radioactivity	Bq	Ci	1 Ci = 3.7×10^{10} Bq
The dose of radiation	The amount of radiation	C/kg	R	1 R = 2.58×10^{-4} C/kg
	The dose of radiation absorbed in living tissue	Gy	rad	1 rad = 0.01 Gy
	Relative biologic effectiveness	Sv	rem	1 rem = 0.01 Sv

Table 1　　　Units for measuring ionizing radiation.

4. Result and Discussion

4-1. Characterization of CdS, CdSe, CdTe and ZnS nanoparticles

4-1-1. The X-ray powder diffraction (XRD) data

The X-ray diffraction patterns confirmed the crystallinites of the sample. Figure 3 shows the X-ray diffraction patterns of the CdS nanoparticles synthesized by γ-irradiation as the change of absorbed dose. The nanoparticles belong to the cubic structure which is also the dominant crystal phase of bulk CdS. Similar nanoparticles were made by Bandarnayake et. al.[20] The as-prepared samples are crystalline as seen by broad XRD features at three prominent lattice planes. The discernible peaks can be indexed to (111), (220), and (311) planes of CdS with cell constant a = 5.811 Å. The structure of CdS is compared with the data from JCPDS file card no. 80-0019. All XRD data have the same planes but the height of peaks slightly change as the change of absorbed dose. When the reactants are not irradiated by γ-irradiation, CdS have few crystallinity.
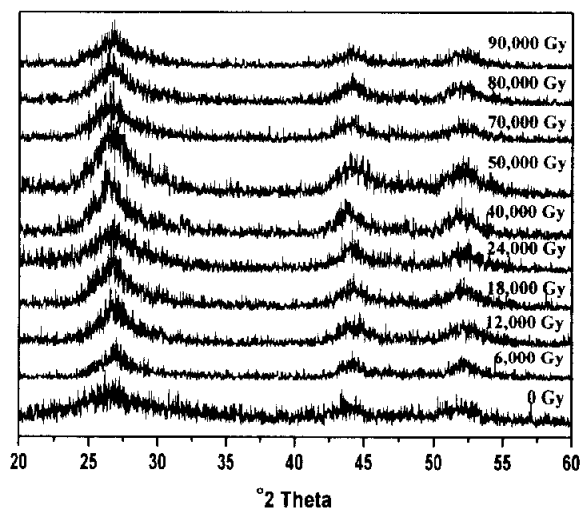
Figure 3   X-ray powder diffraction (XRD) patterns of CdS nanoparticles synthesized by γ-irradiation as the change of absorbed dose.

Figure 4 shows the control of the condition of molar ratio among reactants. Molar ratio among reactants set a standard for Cd^{2+} : oleate = 1 : 2 in Figure 4 (a). Figure 4 (b) - (c) are shown to change the concentration of Cd^{2+} according to the concentration change of oleate. CdS in Figure 4 (b) was not using the oleate as surfactant. That is, CdS was consisted of molar ratio among reactants as Cd^{2+} : oleate = 1 : 0. In Figure 4 (c), CdS was consisted of molar ratio between reactants as Cd^{2+} : oleate = 1 : 4. The excess oleate has influence on the crystallinity. The crystallinity of the standard are better than changed molar ratio.

Figure 4   X-ray powder diffraction (XRD) patterns of CdS nanoparticles synthesized by γ-irradiation as the change of the concentration of oleate as a surfactant; Molar ratio between reactants as (a) Cd^{2+} : oleate = 1 : 2 (a standard), (b) not using oleate, and (c) Cd^{2+} : oleate = 1 : 4.

Figure 5 shows the control of pH condition of solution. In Figure 5 (a), the pH of solution sets a standard at pH 12.6 as basic solution. Because pH 12.6 is set when oleate was dissolved in water. Figure 5 (b) is shown to change the pH 7 with using diluted HCl solution. The crystallinity of basic solution is better than the crystallinity of neutral condition.
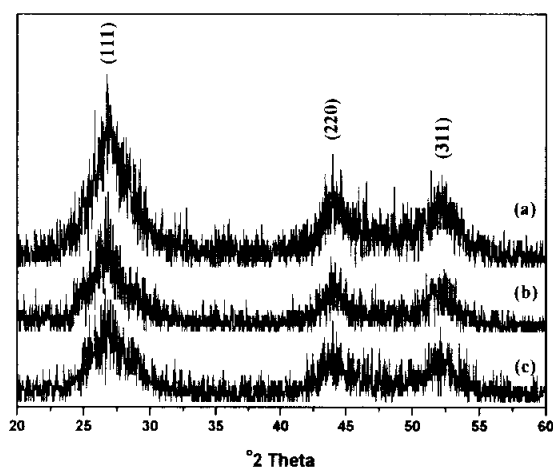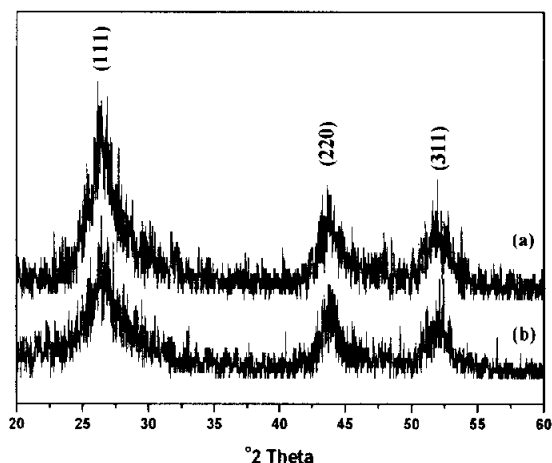
Figure 5   X-ray powder diffraction (XRD) patterns of CdS nanoparticles
                synthesized by γ-irradiation as the change of pH condition;
                (a) pH 12.6 of the solution and (b) pH 7 of the solution.
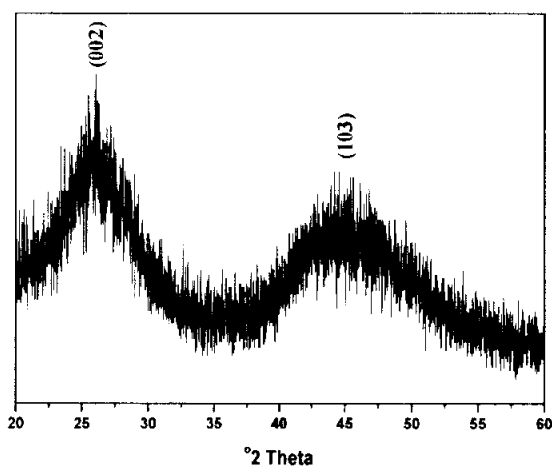
Figure 6   X-ray powder diffraction (XRD) patterns of CdSe nanoparticles
                synthesized by γ-irradiation.

Figure 6 shows the X-ray diffraction spectrum of the CdSe nanoparticles
synthesized by γ-irradiation. Similar features have been observed as broad
XRD peaks in CdSe as those in CdS. It is clear that the X-ray diffraction
spectrum of the CdSe nanoparticles could be indexed to the scattering from

(002) and (103) planes, respectively. CdSe nanoparticle is hexagonal structure. These are corresponding to the structure of CdSe from JCPDS card no. 77-2307.

Figure 7 shows the X-ray diffraction patterns of the CdTe nanoparticles synthesized by γ-irradiation. The discernible peaks can be indexed to (100), (002), and (102) planes of the hexagonal structure of CdTe. These are corresponding to the structure of CdTe from JCPDS card no. 19-0193.

XRD data of ZnS nanoparticles were obtained by γ-irradiation in Figure 8. All the reflections can be indexed to be a pure hexagonal phase with lattice constant a = 3.82 Å and c = 4.93 Å, which are near the reported values. XRD patterns can be indexed to (008), (110), and (118) planes, respectively. The structure of ZnS nanoparticles is compared with the data from JCPDS card no. 39-1363.
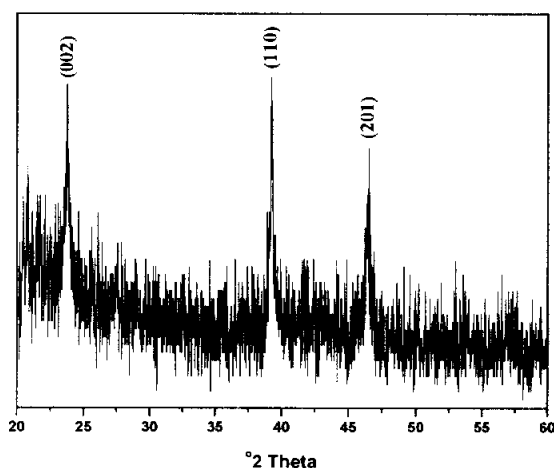

Figure 7   X-ray powder diffraction (XRD) patterns of CdTe nanoparticles synthesized by γ-irradiation.
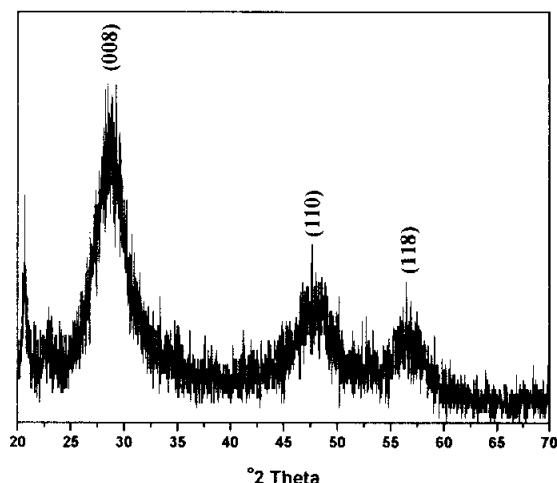
Figure 8   X-ray powder diffraction (XRD) patterns of ZnS nanoparticles
                synthesized by γ-irradiation.

4-1-2. Transmission electron microscopy (TEM)

Transmission electron microscopy (TEM) image is used for the determination of the morphology and size of particles. According to gently irradiated γ-ray, particles grow slowly into larger particles. Particle growth appears to be consistent with "Ostwald ripening",[1,12,51] where the higher surface free energy of small particles makes them less stable with respect to dissolution on the solvent than larger particles. The net result of this stability gradient within a dispersion is slow diffusion of material from small particles. All samples were prepared by evaporation of solvent after the colloidal solution dropping onto a 300 mesh Cu grid.

A drop of CdS nanoparticle in water was placed on the grid and dried in air. The reactants were not irradiated by γ-irradiation in Figure 9 (a). The particles are the distorted shape. TEM image of Figure 9 (b) shows that CdS nanoparticle synthesized by γ-irradiation with a dose of 24,000 Gy. CdS nanoparticles have an irregular ball-shape and the wide size distribution. The size of CdS nanocrystallines has been determined as approximately average

diameter of 9 nm from the TEM image as Figure 9 (b). With increasing absorbed dose, the sizes of CdS nanoparticles were obtained as larger than the sizes of the previous one of Figure 9 (b) and the distorted shape was changed to the ball-shape. Figure 9 (c) shows CdS nanoparticles with average diameter of 24 nm prepared by γ-irradiation with a dose of 70,000 Gy. CdS particles with a dose of 70,000 Gy have relatively narrow size distribution than the sizes of the previous one of Figure 9 (b). The nanoparticles were prepared as the size range of about average 34.4 nm by γ-irradiation with a dose of 90,000 Gy as shown in Figure 9 (d). In the previous paper using γ-irradiation,[50-51,54,59] TEM images of CdS nanoparticles showed only the aggregated state. But the presence of surfactant, such as oleate on the synthesis of CdS nanoparticles, was obtained well dispersed state as one particle as Figure 9.

Figure 10 shows TEM photographs by the change of the concentration of oleate during the synthesis by γ-irradiation with a dose of 50,000 Gy. CdS was synthesized on high concentration of oleate. CdS was synthesized under the molar ratio among reactants as Cd^{2+} : oleate = 1 : 4. According to the increase of oleate, the shape of particles is distorted and the size distribution of particles are very wide as 10.2 - 43 nm. This is interpreted as oleate of the excessive amount interrupted the reaction between Cd^{2+} ions and S^{2-} ions.

TEM images in Figure 11 show the synthesized CdSe nanoparticle by γ-irradiation. A drop of CdSe nanoparticles in iso-octane was placed on the grid and dried in air. CdSe nanoparticles are irregular spherical shape. Figure 11 (a) is CdSe nanoparticles by γ-irradiation with a dose of 30,000 Gy. The diameter of CdSe nanoparticles has been determined as 5 - 10 nm. CdSe nanoparticles were prepared as the size range of 30 - 52 nm by γ-irradiation with a dose of 50,000 Gy as shown in Figure 11 (b). Figure 11 (c) shows CdS nanoparticles with diameter of 28 - 60 nm prepared by γ-irradiation with a dose of 90,000 Gy.

Figure 9   Transmission electron microscopy (TEM) images of CdS nanoparticles synthesized by γ-irradiation as the change of absorbed doses (a) no irradiation (b) 24,000 Gy, (c) 70,000 Gy, and (d) 90,000 Gy.
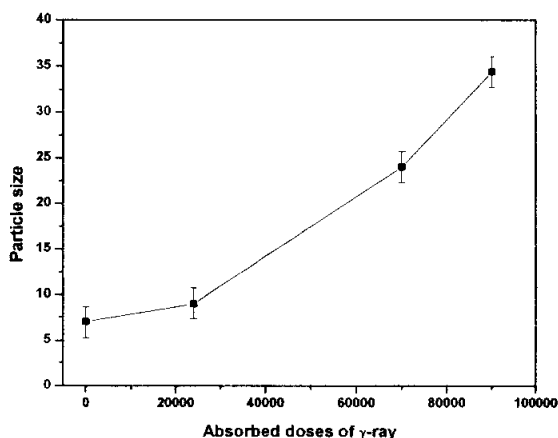
Figure 10   Diagram on the size distribution of CdS nanoparticles synthesized by γ-irradiation as the change of absorbed doses (a) no irradiation (b) 24,000 Gy, (c) 70,000 Gy, and (d) 90,000 Gy.

Figure 10 shows the diagram of CdS nanoparticles that were synthesized by γ-irradiation as the change of absorbed doses. With increasing absorbed dose, the sizes of CdS nanoparticles are much larger in Figure 10. It shows the same result of TEM images in Figure 9.

(a)   (b)

Figure 11   Transmission electron microscopy (TEM) images of CdS nanoparticles synthesized by γ-irradiation as the change of the concentration of oleate as a surfactant; Molar ratio between reactants as (a) Cd^{2+} : oleate = 1 : 2 (a standard) and (b) Cd^{2+} : oleate = 1 : 4.
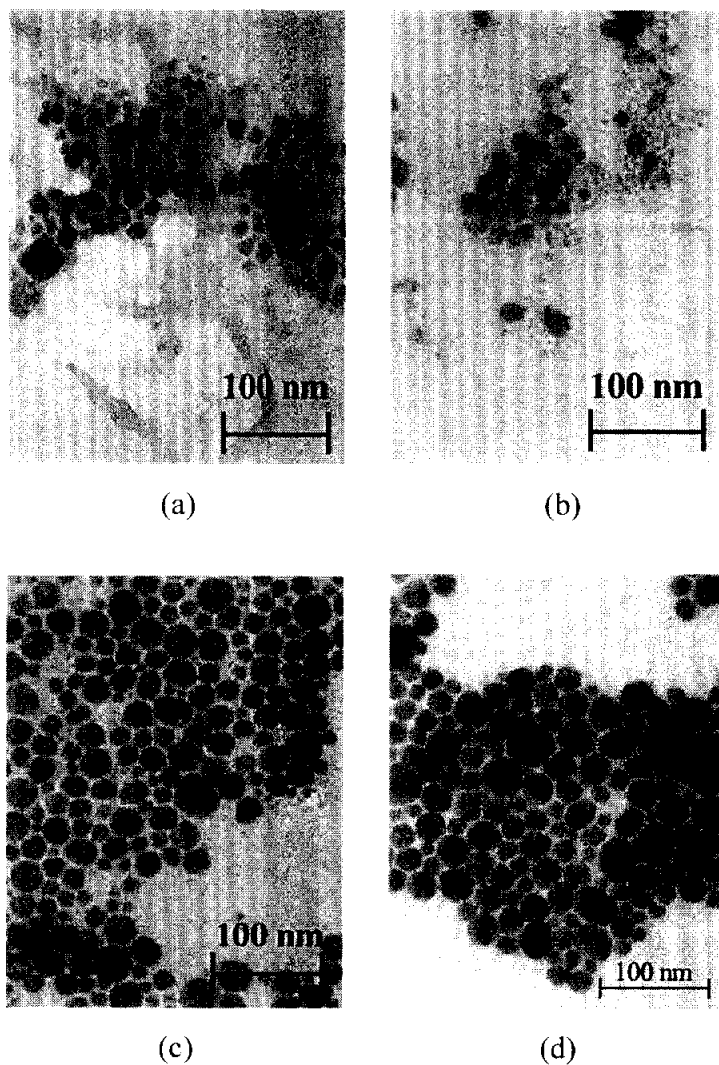
Figure   12   Transmission electron microscopy (TEM) images of CdSe
                   nanoparticles synthesized by γ-irradiation as the change of
                   absorbed doses of (a) 30,000 Gy, (b) 70,000 Gy, and (c)
                   90,000 Gy.

Figure   13   Transmission electron microscopy (TEM) image of CdTe
                   nanoparticles synthesized by γ-irradiation with a dose of
                   90,000 Gy.

Figure 13 is TEM image of CdTe nanoparticles by γ-irradiation with a dose of 90,000 Gy. A drop of CdTe nanoparticle in *iso*-octane was placed on the grid and dried in air. TEM image shows that CdTe nanoparticle synthesized by γ-irradiation has the irregular spherical shape. The diameter of CdTe nanocrystallines has been determined as 29 nm from the TEM image as Figure 13.

100 nm

(a)

100 nm
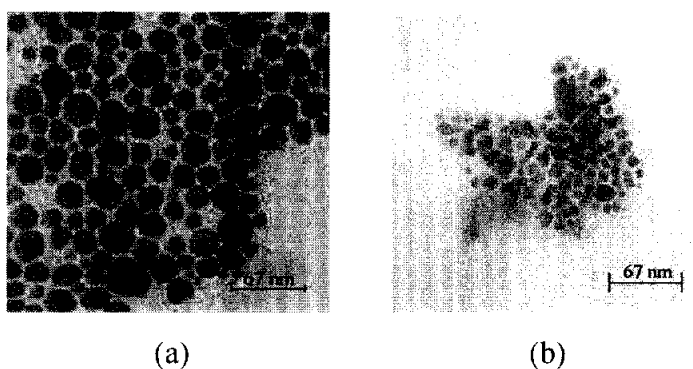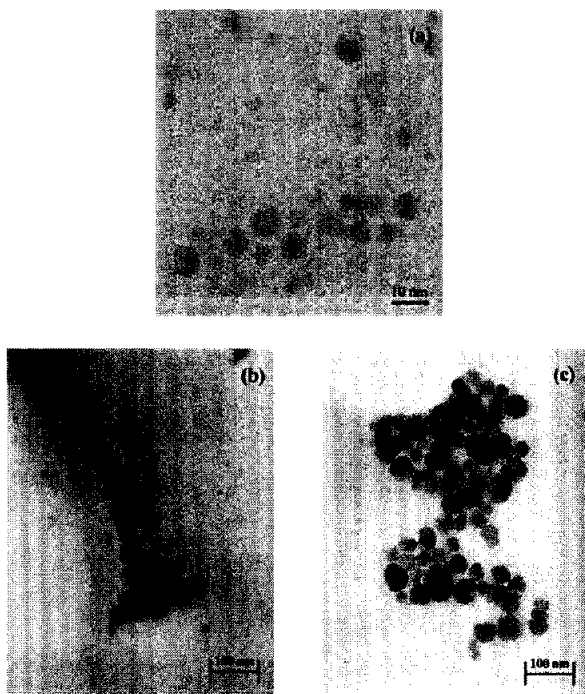
(b)

100 nm

(c)

100 nm

(d)

Figure 14   Transmission electron microscopy (TEM) images of ZnS nanoparticles synthesized by γ-irradiation as the change of absorbed doses of (a) 30,000 Gy, (b) 50,000 Gy, (c) 70,000 Gy, and (d) 90,000 Gy.
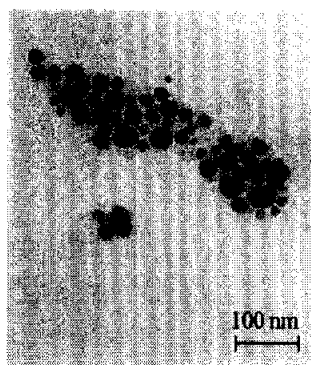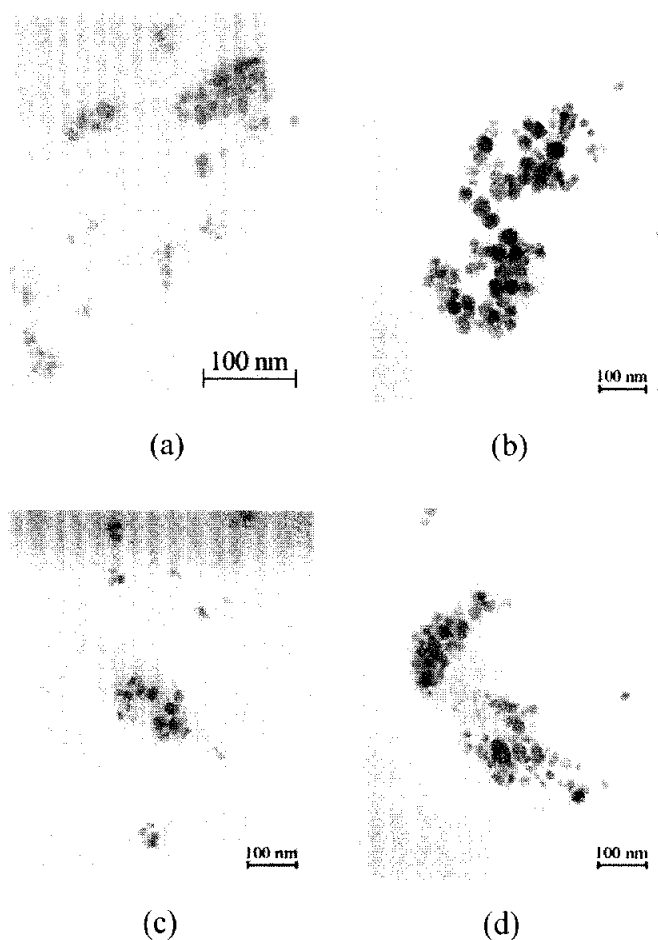
A drop of ZnS nanoparticle in *iso*-octane was placed on the Cu grid and dried in air. TEM image of Figure 14 (a) shows that ZnS nanoparticles synthesized by γ-irradiation with a dose of 30,000 Gy. ZnS nanoparticles have an irregular ball-shaped. The diameter of ZnS nanocrystallines has been determined as approximately 4.9 - 9.8 nm from the TEM image of Figure 14 (a). With an increased dose of γ-ray, the sizes of ZnS nanoparticles were larger than the sizes of the previous one of Figure 14 (a). Figure 14 (b) shows ZnS nanoparticles with 8.7 - 15.3 nm of diameter prepared by γ-irradiation with a dose of 50,000 Gy. ZnS particles with a dose of 70,000 Gy have 10.5 - 16.8 nm of diameter in Figure 14 (c). ZnS nanoparticles were prepared as the size range of 11 - 19.7 nm by γ-irradiation with a dose of 90,000 Gy as shown in Figure 14 (d).

4-1-3. High resolution transmission electron microscopy (HR-TEM)

High-magnification imaging with lattice constant allows the determination of individual crystallite morphology. The existence of lattice planes on the HR-TEM image further confirmed the crystallinity of nanoparticles. In Figure 15 (a), CdS lattice spacing of 3.48 Å was consistent with the lattice spacing of (111) plane. HR-TEM images in Figure 15 (b) and (c) show the lattice of CdTe by γ-irradiation with a dose of 90,000 Gy. CdTe lattice for one particle was observed carefully as 2.2 Å and 3.69 Å. CdTe lattice spacing was consistent with the lattice spacing (110) and (002) planes, respectively. With a dose of 90,000 Gy, the lattice of ZnS is 3.7 Å as Figure 15 (d). ZnS lattice spacing was consistent with the lattice spacing (008) planes.
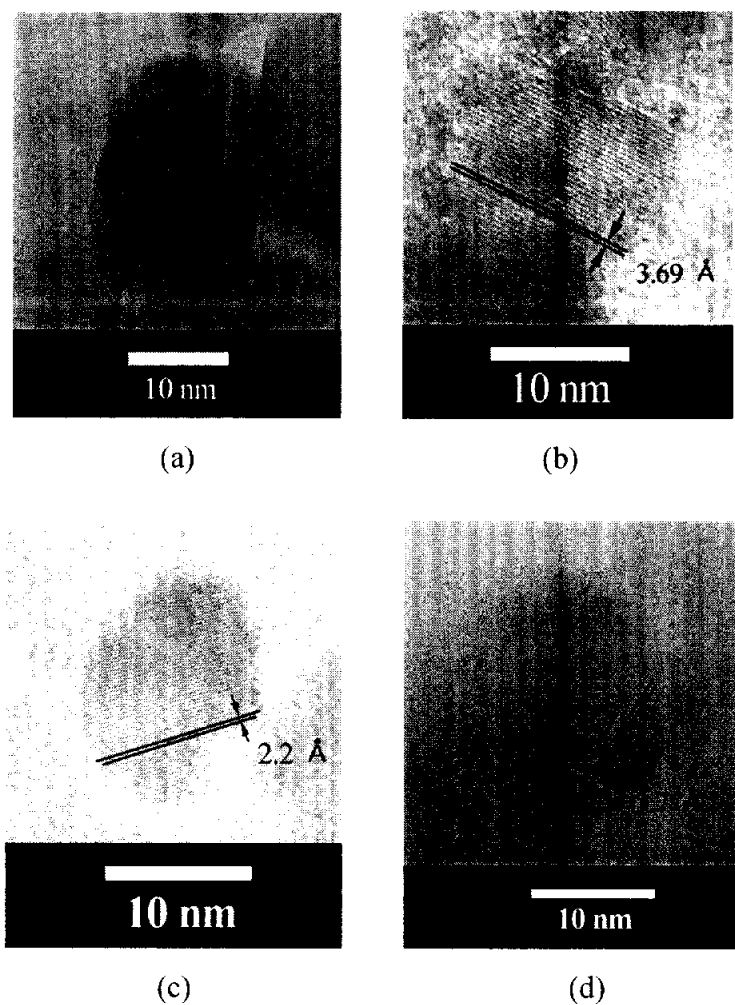
Figure 15   High resolution transmission electron microscopy (HR-TEM) lattice images of (a) of CdS, (b), (c) of CdTe and (d) of ZnS nanoparticles synthesized by γ-irradiation with dose of 90,000 Gy.

3-1-4. Electron diffraction (ED)

Electron diffraction (ED), in its simplest application, is used to identify crystallinity of substances based on the spacing of atomic planes within their structures. ED provides similar structural information as XRD diffraction.

Figure 16 shows an example of electron diffraction patterns from CdS, CdSe and ZnS nanoparticles. From the rich information in this pattern. In Figure 16 (a), the diffraction rings can be indexed to (111), (220) and (311) planes at CdS nanoparticle corresponding to XRD data of CdS. The case of the obtained data was indexed to (002) and (103) planes in CdSe nanoparticles. The same result is observed for XRD spectrum of Figure 6. Figure 16 (c) shows the diffraction rings that can be indexed to (111), (220) and (311) planes at ZnS nanoparticle corresponding to XRD data of ZnS.

Figure 16   Electron diffraction (ED) patterns of (a) CdS, (b) CdSe, and (c) ZnS nanoparticles.

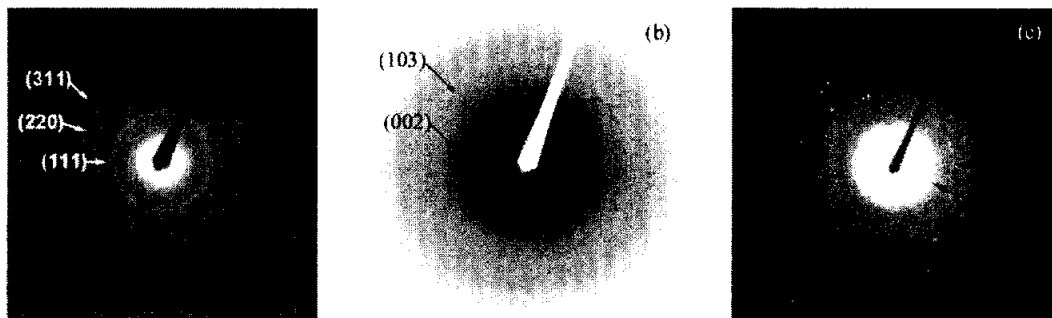## 3-1-5. Energy dispersive X-ray (EDX) spectrometer study

The elemental composition of nanoparticles was analyzed by EDX. Figure 17 shows the EDX spectra of the CdS, CdSe, CdTe, and ZnS nanoparticles. Peaks for the elements Cd and S were observed in Figure 17 (a). An EDX spectum of CdS shows that clear peaks of Cd and S were detected. The presence S and Cd elements could be confirmed at 2.25 keV and 3.07 keV in the EDX spectrum, respectively. The EDX measurement indicates the presence of Cd and S in samples, with the Cd : S ratios 50.31 : 49.69 being very close to 1 : 1. In CdSe nanoparticles, the EDX analysis indicates that the elemental Cd is present at 3.07 keV. And Se Lα1, Se Lβ1, Se Kα1 and Se Kβ1 are presented at 1.37 keV, 1.41 keV, 10.95 keV and 12.16 keV. Element analysis for the samples of CdSe gives Cd : Se atomic ratios 36.44 : 63.56, which is close to 1 : 1. There is no impurity atom of the nanocrystallites. Peaks for the elements Cd and Te were observed in Figure 17 (c). The presence of Te Lα1 and Te Lβ1 could be shown at 3.67 keV and 3.93 keV in the EDX spectrum. And Cd Lα1 element could be confirmed at 3.07 keV. The EDX measurement indicates the presence of Cd and Te in samples, with the Cd : Te ratios 48.94 : 51.06 being very close to 1:1. In Figure 17 (d), An EDX spectum of ZnS shows that clear peaks of Zn and S were detected. The presence S and Zn elements could be confirmed at 2.25 keV and 0.9 keV, 8.4 keV, and 9.3 keV in the EDX spectrum, respectively. Elemental analysis for the sample of ZnS gives Zn : S atomic ratios 48.98 : 51.02, which is close to 1:1. There is no impurity atom of the nanocrystallites. From the electron diffraction pattern and the EDX spectra, we could confirm that the CdS, CdSe, CdTe, and ZnS nanoparticles are pure materials.
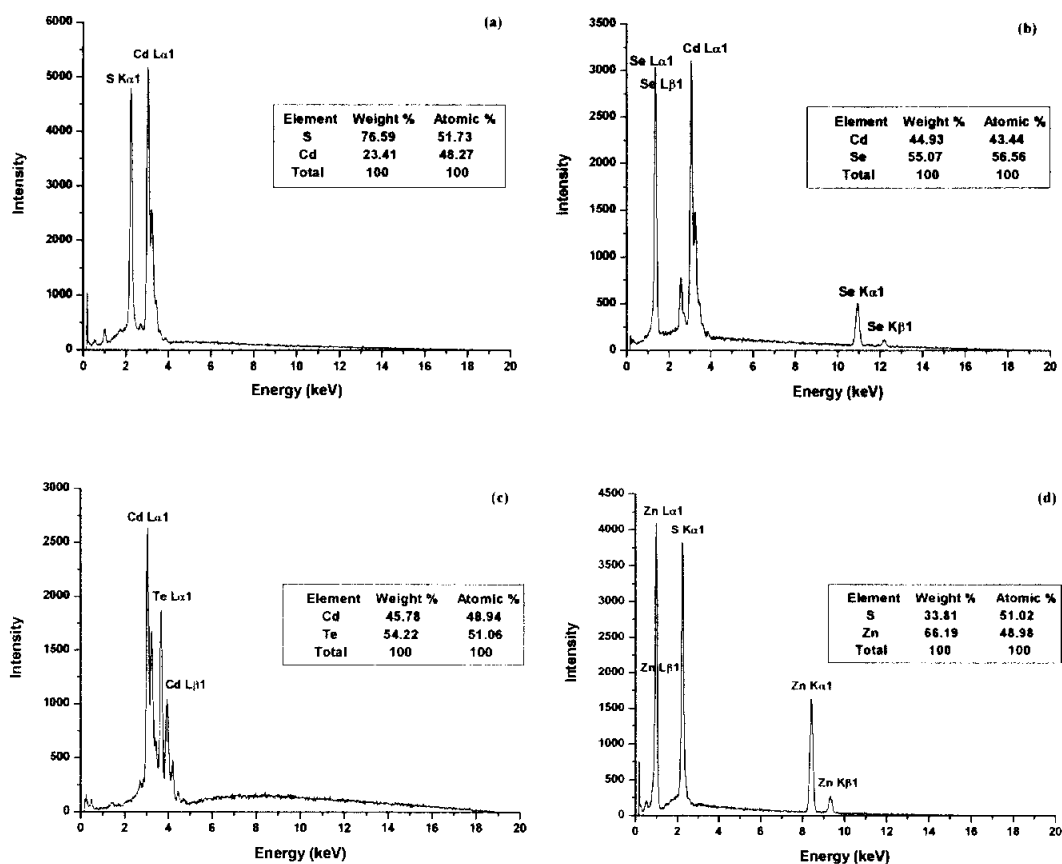
Figure 17   Energy dispersive X-ray (EDX) spectra of (a) CdS, (b) CdSe, (c) CdTe, and (d) ZnS nanoparticles.

3-1-5. X-ray photoelectron spectroscopy (XPS) analysis

The elemental analysis and binding energy of CdS nanoparticles was analyzed by XPS. The sample was prepared directly on the pretreated Al Kα radiation as exciting source. Figure 18 shows the XPS spectra for CdS nanoparticles with a dose of 90,000 Gy by γ-irradiation. The result of Cd3d$_{5/2}$, Cd3d$_{3/2}$ and S2p electron binding energies are shown Figure 18. The appearance of the characteristic XPS peaks of Cd3d$_{5/2}$ and Cd3d$_{3/2}$ at 402.5 eV and 409.3 eV, S2p peak at 158.95 eV confirmed the existence of cadmium and sulfur species in the particles. The oxidation state of cadmium ion within CdS nanoparticles is known to strongly affect the electronic energy structure and transition probabilities responsible for optical properties. These data indicate the amount of Cd^{2+} ions. Elemental analysis for the samples of CdS in Figure 18 gives Cd : S atomic ratios as 51.23 : 48.77, which is close to 1 : 1.

Electron level	Binding energy (eV)	Valency
Cd3d$_{5/2}$	402.5	+2
Cd3d$_{3/2}$	409.3	
S2p	158.95	-2

Table 2   Binding energies and valent states of the product.
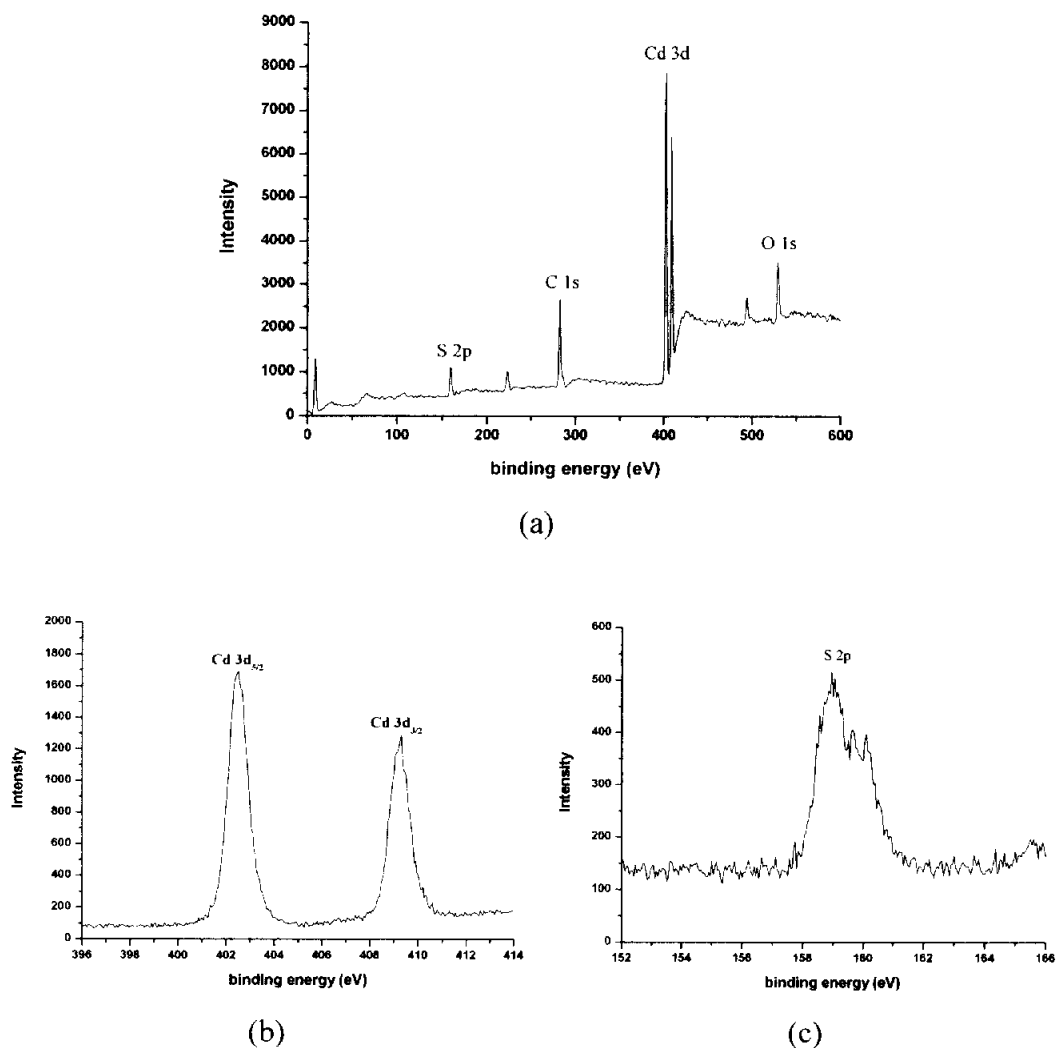
(a)

(b)

(c)

Figure 18   X-ray photoelectron spectroscopy (XPS) analysis of CdS nanoparticles prepared by γ-irradiation with a dose of 90,000 Gy; (a) typical XPS survey spectrum, (b) close-up surveys for Cd3d core, and (c) close-up surveys for S2p core.

3-1-5. The Optical property

As shown in Figure 19, the CdS nanoparticles exhibit a well-defined absorption feature around 475 nm, which is considerably blue-shifted relative to the bulk band gap for hexagonal CdS crystals (515 nm),[2-3] indicating quantum size effect. As the absorption spectra of solutions irradiated by the different irradiation doses, the absorption spectra were shown to be changed. CdS nanoparticle synthesized by γ-irradiation with a dose of 30,000 Gy indicated absorption peak at about 468 nm. Figure 19 (b) shows CdS nanoparticles synthesized by γ-irradiation with a dose of 70,000 Gy. This peak appeared at 476 nm. The absorption peak of CdS nanoparticles prepared by γ-irradiation with a dose of 90,000 Gy appeared at 489 nm. Also the absorption spectra of CdS nanoparticles were red-shifted with increasing absorbed doses of γ-ray due to increasing particle size.

Figure 19   UV-vis spectra of CdS nanoparticles synthesized by γ-irradiation as the change of absorbed doses of (a) 30,000 Gy, (b) 70,000 Gy, and (c) 90,000 Gy.

As the absorption spectra of CdSe nanoparticles irradiated by the different irradiation doses, the absorption spectra were shown to be changed. CdSe nanoparticle synthesized by γ-irradiation with a dose of 30,000 Gy indicated absorption peak at about 414 nm. The absorption peak of CdSe nanoparticles prepared by γ-irradiation with a dose of 70,000 Gy appeared at 423 nm. Also the absorption spectra of CdSe nanoparticles were red-shifted with increasing absorbed doses due to increasing particle size. Figure 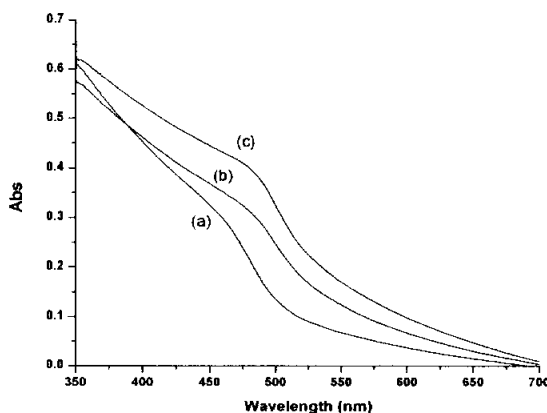20 (b) shows the absorption spectra of CdSe nanoparticles synthesized by γ-irradiation with a dose of 70,000 Gy. In Figure 20 (c), CdSe nanopartcles exhibit a well-defined absorption feature at 442 nm.

Figure   20   UV-vis spectra of CdSe nanoparticles synthesized by γ-irradiation
            as the change of absorbed dose; of (a) 30,000 Gy, (b) 70,000
            Gy, and (c) 90,000 Gy.

Figure 21 displays the absorption spectra of ZnS nanoparticles. As shown in Figure 21, this is a blue-shifted from the bulk ZnS material of which was usually appeared at 310 - 318 nm. ZnS nanoparticles synthesized by γ-irradiation with a dose of 30,000 Gy indicated absorption peak at about 310 nm. The absorption peak of ZnS nanoparticles prepared by γ-irradiation with a dose of 70,000 Gy appeared at 314 nm. Also the absorption spectra of ZnS

nanoparticles were red-shifted with increasing absorbed dose of γ-ray due to increasing particle size. Figure 21 (b) shows the absorption spectra of ZnS nanoparticles synthesized by γ-irradiation with a dose of 70,000 Gy. ZnS nanopartcles exhibit a well-defined absorption feature at 318 nm in Figure 21 (c).
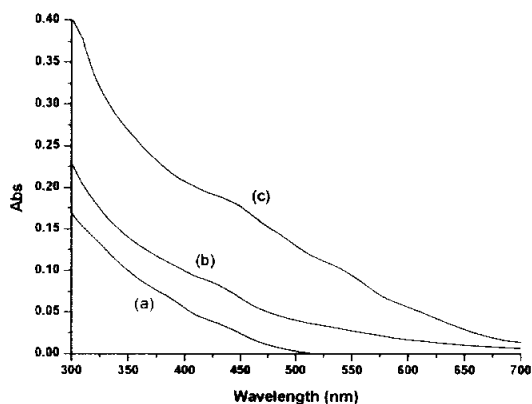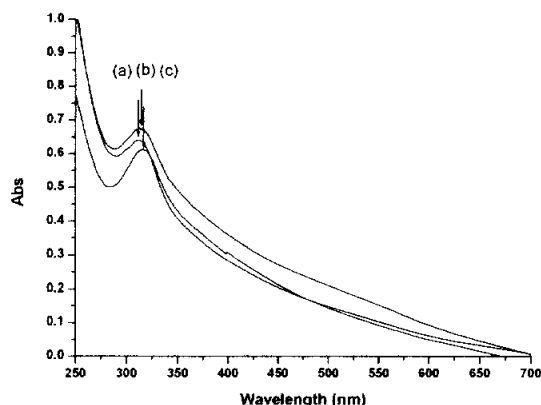

Figure 21 UV-vis spectra of ZnS nanoparticles synthesized by γ-irradiation as the change of absorbed doses of (a) 30,000 Gy, (b) 70,000 Gy, and (c) 90,000 Gy.

The optical properties of as-prepared products including the synthesized CdS, CdSe, and CdTe nanoparticles were studied with photoluminescence spectra as Figure 22. The spectrum of CdS with a dose of 90,000 Gy shows the wide peaks at 500 - 650 nm in Figure 22 (a). The CdS nanoparticle synthesized by γ-irradiation shows a green color. Photoluminescence spectrum of CdSe shows emission band at the wavelength range of 570 - 700 nm. Figure 22 (c) shows the spectrum of CdTe with a dose of 90,000 Gy. This shows the emission band at the wavelength of 560 - 700 nm. The synthesized CdS, CdSe, and CdTe nanoparticles were in the size quantization regime and showed a well-developed size-dependant maximum near the absorption onset, which was

ascribed to the excitonic transition.
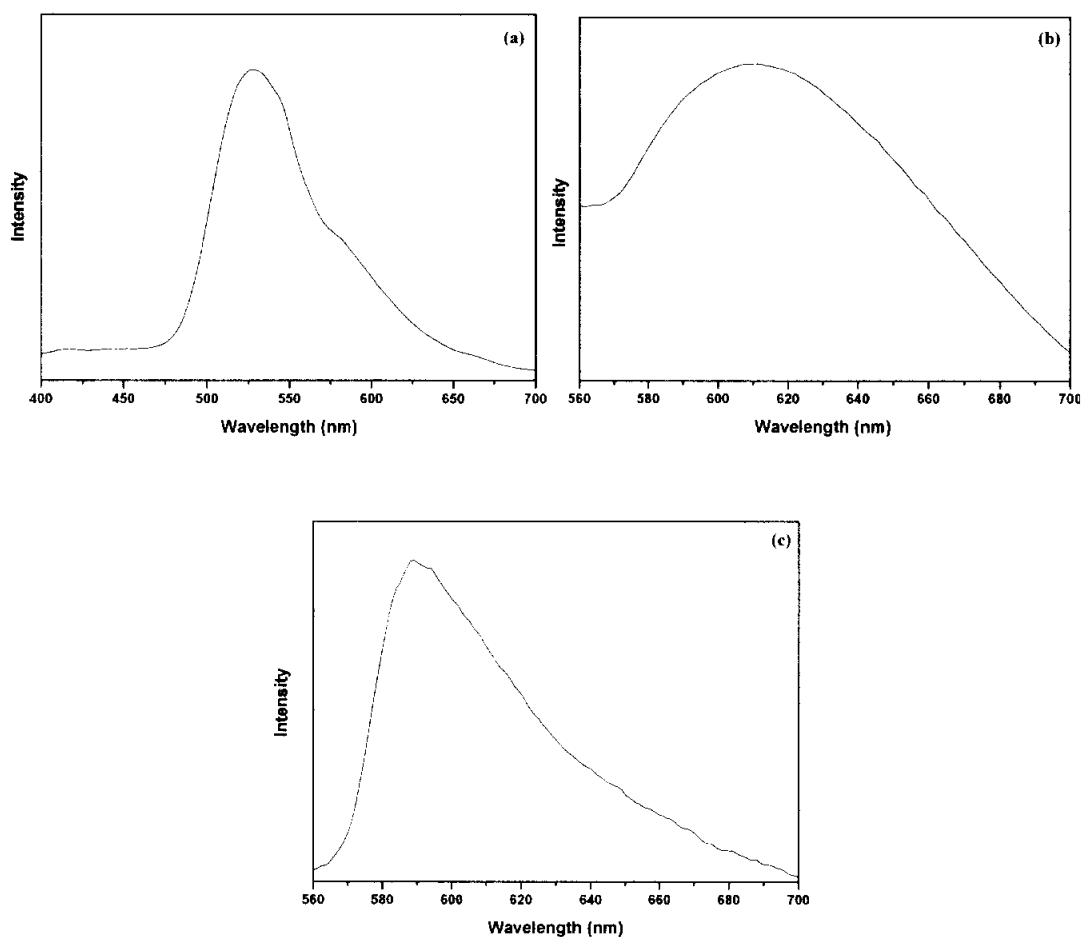

Figure 22. Photoluminescence spectra for the synthesized CdS nanoparticles dispersed in water, λ_{exc} = 365 nm (a), the synthesized CdSe nanoparticles dispersed in chloroform, λ_{exc} = 365 nm and the synthesized CdTe nanoparticles dispersed in chloroform, λ_{exc} = 265 nm.

4-2. Characterization of CdS, CdSe, CdTe and ZnS nanorods and nanowires synthesized by γ-irradiation

The whole process can be expressed as follows:[36-38,60]

$$Cd(en)_3^{2+} + S^{2-} \rightarrow CdS(en)_m \leftrightarrow CdS(en)_{m-n} + n(en)$$

$$(en = ethylenediamine)$$
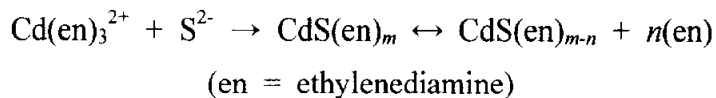
First, Cd^{2+} ion coordinated with en molecule to form $Cd(en)_3^{2+}$. Then, the reaction between $Cd(en)_3^{2+}$ and S^{2-} produced CdS powder with its surface-adsorbed en molecules. Meanwhile, the conformation of the en molecule coordinated with Cd^{2+} changed from the gauche to the trans conformation. However, the interaction between the en molecules and Cd^{2+} on the surface of CdS was weak when the en molecule was in the trans conformation. Therefore, this structure was destroyed by γ-irradiation. This dissociation of the en molecules from the surface of CdS resulted in the evolution process of the morphology along with one axis. In fact, the en molecule in the trans conformation acted as an intermediate. In py, the principle of the reaction is similar to that of en.

4-2-1. The X-ray powder diffraction (XRD) data

These peaks are distinguished from the peaks of cubic CdS nanoparticles that only have the diffraction peak of (111), (220) and (311)[12]. That is, the phase was changed from cubic structure to hexagonal structure by using ed. However, there is a bit stronger (002) peak in the XRD patterns than expected from the powder patterns. Figure 23 shows the X-ray diffraction patterns of the CdS nanorods and nanowires synthesized by γ-irradiation with a dose of 90,000 Gy. CdS nanorod havs different peak positions from CdS nanowires.

The discernible peaks can be indexed to (100), (002), (101), (110), (103), and (201) planes of the hexagonal structure of CdS with cell constant a = 4.136 Å and c = 6.713 Å as Figure 23 (a). The structure of CdS is compared with the data from JCPDS file card no. 06-0314. On the other hand, the XRD data of CdS nanowires were different from that of CdS nanorods. CdS nanowires have cubic structure from JCPDS file card no. 800-0019. But CdS nanowires didn't remove impurities like sodium sulfite (Na_2SO_3).

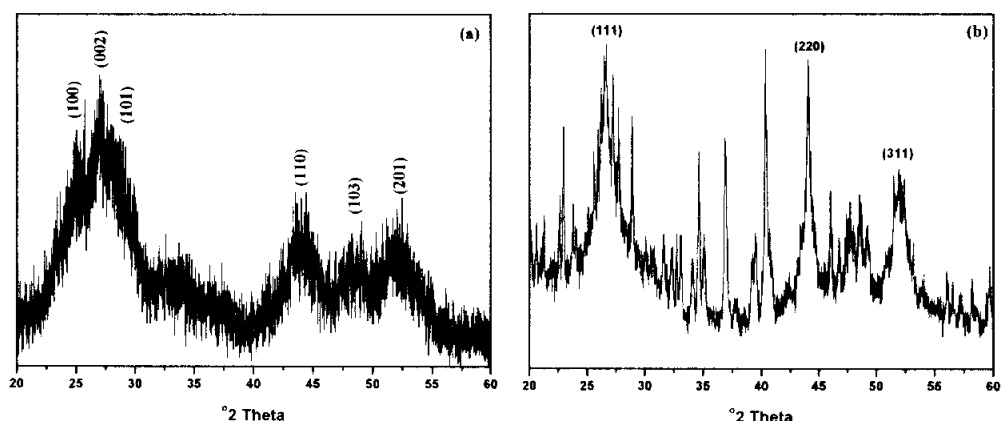Figure 23   XRD patterns of CdS nanorods (a) and nanowires (b) synthesized by γ-irradiation with a dose of 90,000 Gy.

Figure 24   XRD patterns of CdSe nanorods (a) and nanowires (b) synthesized by γ-irradiation with a dose of 90,000 Gy.

Figure 24 shows the X-ray diffraction patterns of the CdSe nanorods and nanowires synthesized by γ-irradiation with a dose of 90,000 Gy. The discernible peaks can be indexed to (100), (002), (101), (110), (103), and (112) planes of the hexagonal structure of CdSe with cell constant a = 4.29 Å and c = 1.6306 Å as Figure 24. CdSe nanowires are corresponded with the spectrum from JCPDS file card no. 77-2307.

Figure 25   XRD patterns of CdTe nanorods (a) and nanowires (b) synthesized by γ-irradiation with a dose of 90,000 Gy.
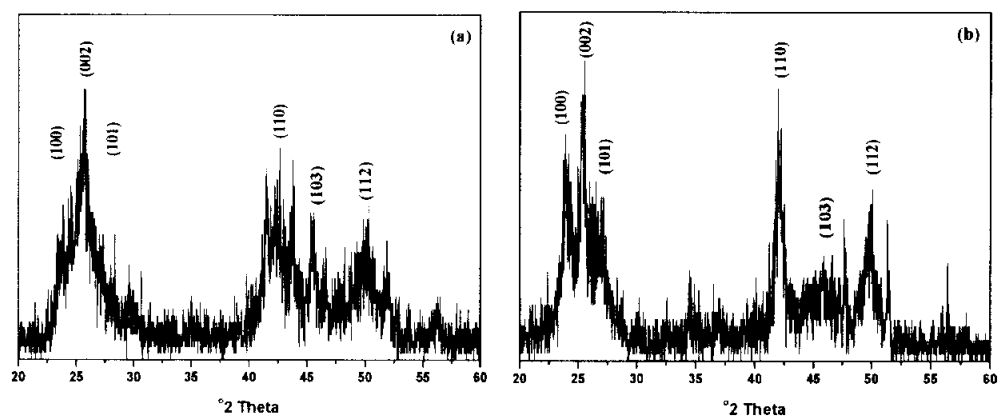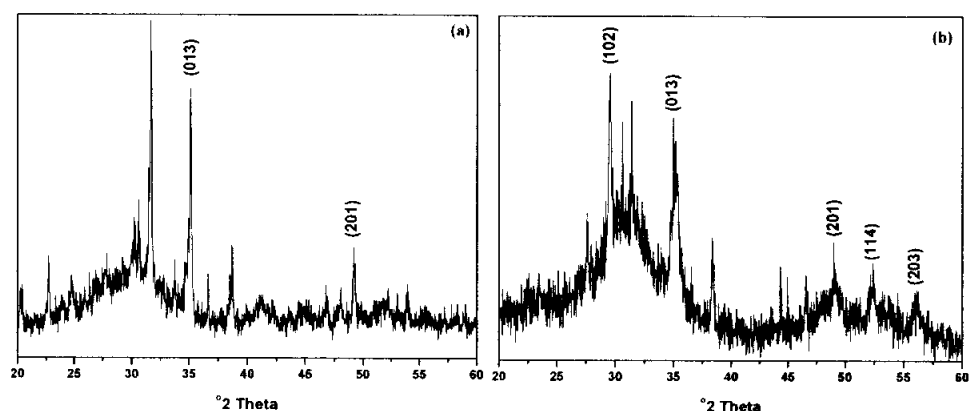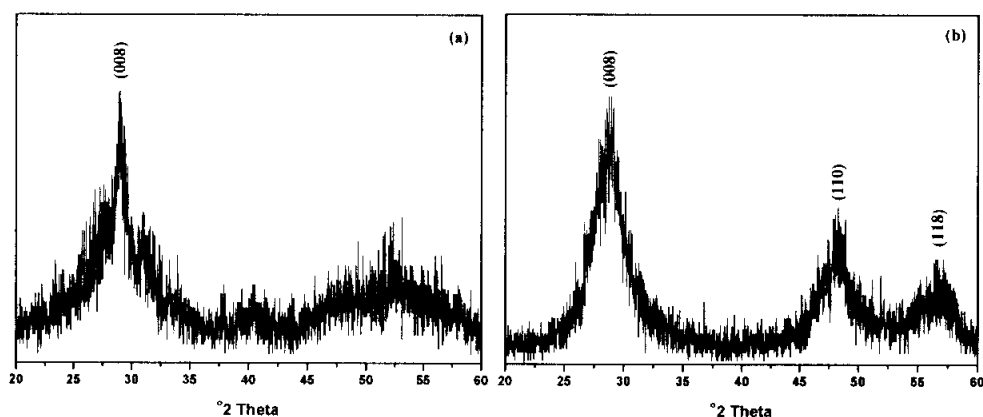

Figure 26   XRD patterns of ZnS nanorods (a) and nanowires (b) synthesized by γ-irradiation with a dose of 90,000 Gy.

Figure 25 shows the X-ray diffraction patterns of the CdTe nanorods and nanowires synthesized by γ-irradiation with a dose of 90,000 Gy. CdTe nanorods and nanowires have the hexagonal structure with cell constant a = 4.292 Å and c = 10.235 Å as Figure 25. CdTe nanorods and nanowires are corresponded with the spectrum from JCPDS file card no. 82-0474. But the samples of CdTe nanorods and nanowires still have some impurities like sodium and tellurium.

Figure 26 shows the X-ray diffraction patterns of the ZnS nanorods and nanowires synthesized by γ-irradiation with a dose of 90,000 Gy. ZnS nanorods have a different peak position from ZnS nanowires.

4-2-2. Transmission electron microscopy (TEM)

As-prepared CdS, CdSe, CdTe, and ZnS powders in polyamines such as ethylenediamine and pyridine display rodlike and pearl necklace morphology[43] with diameters of several nanometers and lengths of up to several microns. Semiconducting materials have shown the different shape to be synthesized in the different solvent.[36-38,60] The growth of CdS nanorods was oriented along with one axis and morphologies were 1D rodlike. Figure 27 (a) shows TEM micrograph of as-prepared CdS nanorods in ethylenedaimine. They have width of about 120 nm and length of about 600 nm. CdS synthesized in pyridine has a different shape of CdS synthesized in ethylnedamine. CdS synthesized in pyridine shows the shape of necklace and have as the diameter of 38 nm. CdS nanowires appeared to be agglomerates of smaller particles. With irradiated to the reactants by γ-irradiation, CdS cluster have self-assembled and formed nanowires. The diameter of nanowires was decided on the size of nanoparticles. Figure 27 (c) shows TEM image of CdSe synthesized in pyridine by γ-irradiation with a dose of 90,000 Gy. The synthesized CdSe existed as the diameter 64 nm scales and shown the pearls. Figure 27 (d) and (e) are TEM micrographs of CdTe synthesized in ethylenediamine and pyridine. Figure 27 (d) shows the morphology of nanorods in ethylenediamine. These nanorods are width of about 22 nm and length of about 210 nm. Figure 27 (e) shows the necklace shape of CdTe nanowires synthesized in

pyridine. CdTe nanowires are width of about 45 nm scales. Figure 27 (f) displays TEM image of ZnS nanowires synthesized in pyridine by γ -irradiation. ZnS nanowires are shown as width of 48 nm and have the pearls. The recrystallization may occur via the Ostwald ripening with intermediate ion transfer from smaller nanoparticles to growing rods and wires in clusters.

(a)　　　　　　(b)　　　　　　(c)

(d)　　　　　　(e)　　　　　　(f)
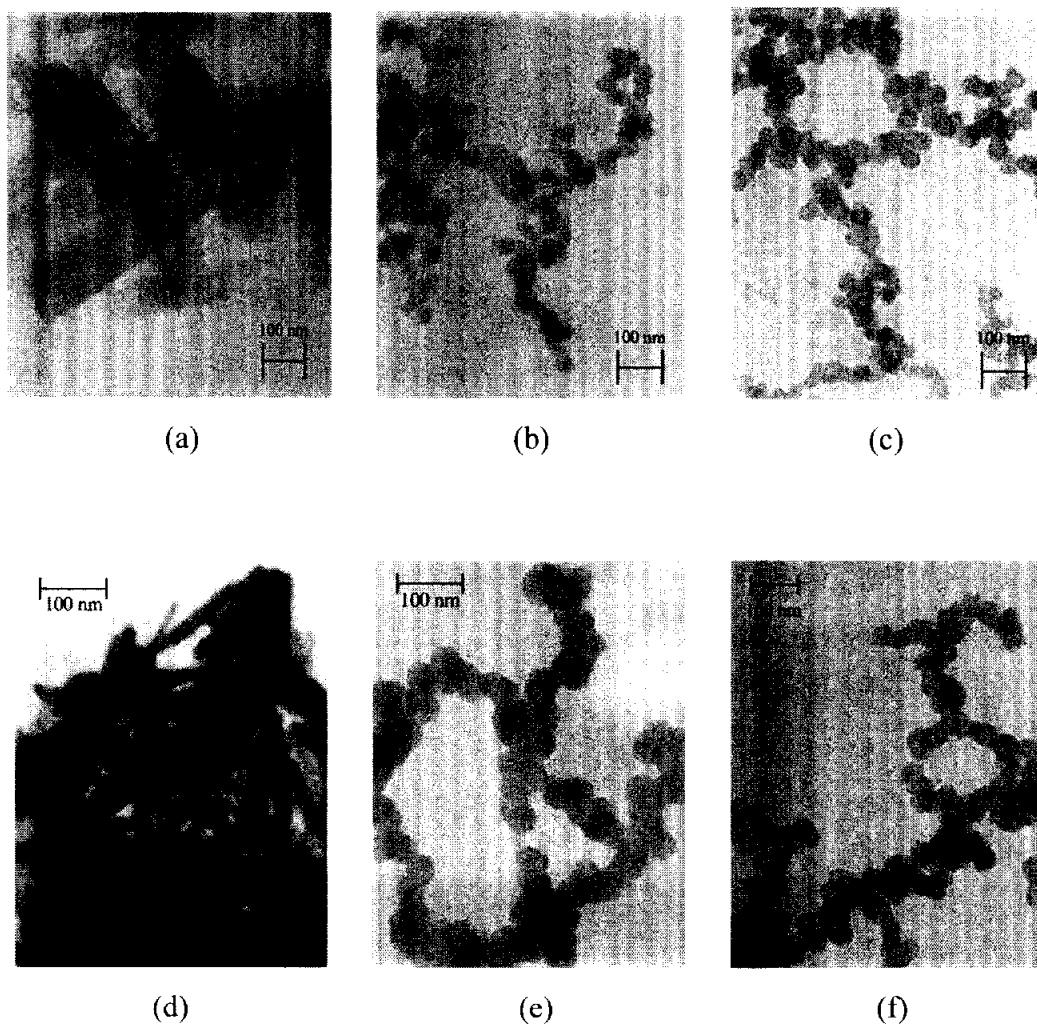
Figure 27　　　Transmission electron microscopy (TEM) images of various nanorods and nanowires synthesized by γ -irradiation with a dose of 90,000 Gy; (a) CdS in ed, (b) CdS in py, (c) CdTe in ed, (d) CdTe in py, (e) CdSe in py, and (f) ZnS in py.

4-2-3. Energy dispersive X-ray (EDX) spectra

Figure 28 shows the EDX spectra of the CdS, CdSe, CdTe, and ZnS nanowires by a SEM. The result of nanowires is similar to nanoparticle. EDX spectra could confirm that the CdS, CdSe, CdTe, and ZnS nanorods are pure materials. CdS, CdSe, CdTe, and ZnS nanowires are similar to molar ratio of those nanorods.

Figure 28   Energy dispersive X-ray (EDX) spectra of (a) CdS, (b) CdSe, (c) CdTe, and (d) ZnS nanowires.

5. Conclusion

Semiconducting materials of CdS, CdSe, CdTe, and ZnS were successfully synthesized by γ-irradiation at room temperature and the atmospheric pressure. Nanoparticles were synt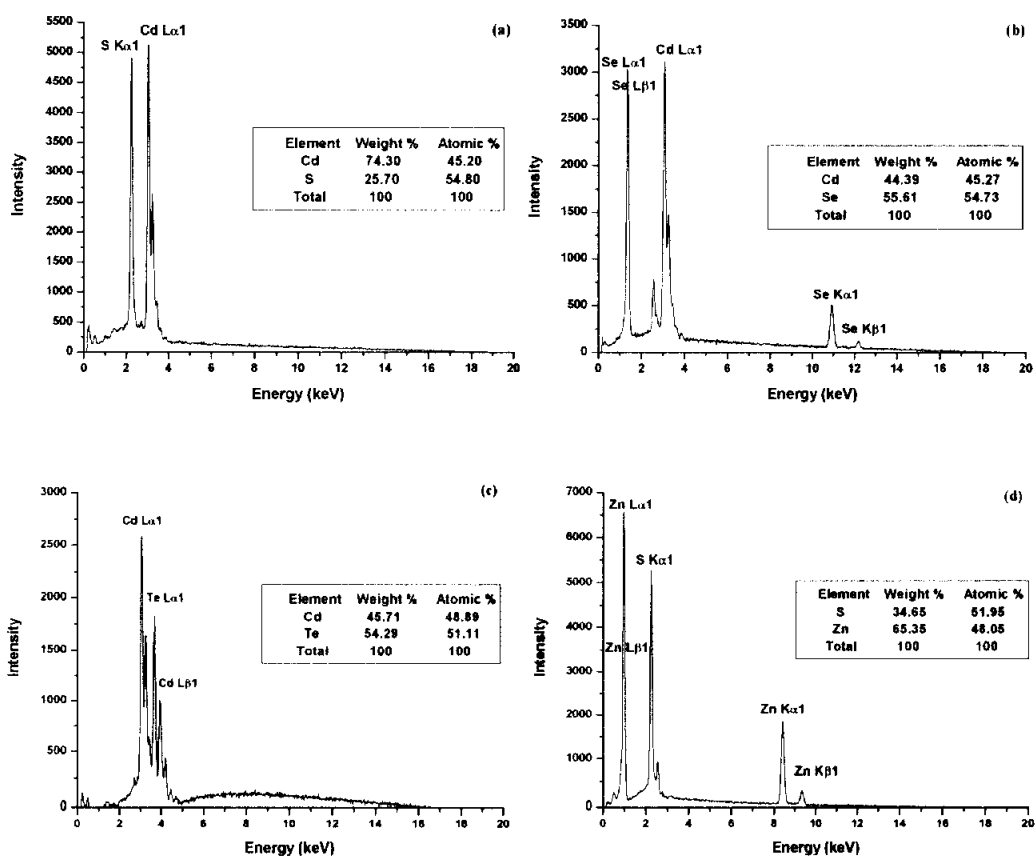hesized in pure water. Also, nanorods and nanowires were prepared in ed and py, the solvent molecules controled the morphology. In XRD data, the synthesized CdS, CdSe, CdTe, and ZnS could be confirmed on the information of the structure and the crystallinity of them. From TEM images, their size and morphology of nanoparticles, nanorods, and nanowires were determined. The crystal planes are searched by ED patterns and HR-TEM images. The elemental analysis was investigated with EDX and XPS spectra. The synthesized nanoparticles show strong band-edge of photoluminescence. PL of the synthesized nanoparticles showed wavelength modification into visible region when excited at UV wavelength. For the structural characterization, sodium oleate was successfully used to replace the surfactant molecules on surface of nanoparticles. UV-visible spectra were shown to investigate the optical properties of the synthesized nanoparticles.

6. References

1.   Alivisatos, A. P. *Science* **1996**, *271*, 933.

2.   O'Brien, P.; Pickett, N. L. *Chem. Master.* **2001**, *13*, 3843.

3.   Reisfeld, R. *Journal of Alloys and Compounds* **2002**, *341*, 56.

4.   Henglein, A. *Chem Rev.* **1989**, *89*, 1861.

5.   Steigerwald, M. L.; Brus, L. E. Acc. *Chem. Res.* **1990**, *23*, 183.

6.   Bawendi, M. G.; Steigerwald, M. L.; Brus, L. E. Annu. *Rev. Phys. Chem.* **1990**, *41*, 477.

7.   Weller, H. *Angew. Chem., Int. Ed. Engl.* **1993**, *32*, 41.

8.   Weller, H. *Adv. Mater.* 1993, *5*, 88.

9.   Hagfeldt, A.; Grätzel, M. *Chem. Rev.* 1995, *95*, 49.

10.   Fendler, J. H.; Meldrum, F. C. *Adv. Mater.* 1995, *7*, 607.

11.   Alivisatos, A. P. *J. Phys. Chem.* 1996, *100*, 13226.

12.   Murray, C. B.; Norris, D. J.; Bawendi, M. G. *J. Am. Chem. Soc.* **1993**, *115*, 8706.

13.   Rossetti, R.; Ellison, J. L.; Gibson, J. M.; Brus, L. E. *J. Chem. Phys.* **1984**, *80*, 4464.

14.   Kortan, A. R.; Hull, R.; Opila, R. L.; Bawendi, M. G.; Steigerwald, M. L.; Carrol, P. J.; Brus, L. E. *J. Am. Chem. Soc.* **1990**, *112*, 1327.

15.   Steigerwald, M. L.; Alivisatos, A. P.; Gibson, J. M.; Harris, T. D.; Kortan, A. R.; Muller, A. J.; Thayer, A. M.; Duncan, T. M.; Douglass, D. C.; Brus, L. E. *J. Am. Chem. Soc.* **1988**, *110*, 3046.

16.   Cowley, A. H.; Jones, R. A. *Polyhedron* **1994**, *13*, 1149.

17.   Bradley, D. C. *Polyhedron* **1994**, *13*, 1111.

18.   O' Brien, P.; Nomura, R. *J. Mater. Chem.* **1995**, *5*, 1761.

19.   Trindade, T.; O' Brien, P. *J. Mater. Chem.* **1996**, *6*, 343.

20.   Bandaranayake. R. J.; Wen, G. W.; Lin, J. Y.; Jiang, H. X.; Sorensen, C. M. *Appl. Phys. Lett.* **1995**, *67*, 831.

21.   Braun, P. V.; Osenar, P.; Tohver, V.; Kennedy, S. B.; Stupp, S. I. *J. Am. Chem. Soc.* **1999**, *121*, 7302.

22. Braun, P. V.; Stupp, S. I. *Materials Research Bulletin* **1999**, *34*, 463.

23. Peng, X.; Manna, I.; Yang, W.; Wickham, j.; Scher, E.; Kadavanich, A.; Alivsatos, A. P. *Nature* **2000**, *404*, 29.

24. Hao, E.; Zhang, H.; Yang, B.; Ren, H.; Shen, J. *Journal of Colloid and Interface Science* **2001**, *238*, 285.

25. Wang, W.; Germanemko, I.; El-Shall, S. M. *Chem. Mater.* **2002**, *14*, 3028.

26. Joo, J.; Na, H. B.; Yu, T.; Yu, J. H., Kim, Y. W.; Wu, F.; Zhang, J. Z.; Hyeon, T. *J. Am. Chem. Soc.* **2003**, *125*, 11100.

27. Kim, S.; Fisher, B.; Eisler, H.; Bawendi, M. *J. Am. Chem. Soc.* **2003**, *125*, 11466.

28. Rogach, A. L. *Materials Science and Engineering B* **2000**, *69-70*, 435.

29. Yang, J.; Yag, X.; Yu, S.; Liu, X.; Qian, Y. *Materials Research Bulletin* **2000**, *35*, 1509.

30. Soliman, M.; Kashyout, A. B.; Shabana, M.; Elgamal, M. *Renewble Energy* **2001**, *23*, 471.

31. Rogach, A. L.; Katsikas, L.; Kornowski, A.; Su, D.; Eychmüller, A.; Weller, H. *Ber. Bunsen-Ges. Phys. Chem.* **1996**, *100*, 1772.

32. Gaponik, N.; Talapin, D. V.; Rogach, A. L.; Hoppe, K.; Shevchenko, E. V., Kornowski, A.; Eychmüller, A.; Weller, H. *J. Phys. Chem. B* **2002**, *106*, 7177.

33. Rogach, A. L.; Kornowski, A.; Gao, M.; Euchmüller, A.; Weller, Horst. *J. Phys. Chem. B* **1999**, *103*, 3065.

34. Guo, M.; Kirstein, S.; Möhwald, H.; Rofach, A. L.; Kornowski, A.; Eychmüllerne, A.; Eychmuller, A.; Weller, H. *J. Phys. Chem.* **1998**, *102*, 8360.

35. Kapitonov, A. M.; Stupak, A. P.; Gaponenko, S. V.; Petrov, E. P.; Rogach, A. L.; Eychmüller, A. *J. Phys. Chem. B* **1999**, *103*, 10109.

36. Yang, J.; Zeng, J.; Yu, S.; Yang, L.; Zhou, G.; Qian, Y. *Chem. Mater.* **2000**, *12*, 3259.

37. Yu, S.; Wu, Y.; Yang, J.; Han, Z.; Xie, Y.; Qian, Y.; Liu, X. *Chem. Mater.* **1998**, *10*, 2309.

38. Li, Y.; Liao, H.; Ding, Y.; Fan, Y.; Zhang, Y.; Qian, Y. *Inorg. Chem.* **1999**, *38*, 1382.

39. Abdelouas, A.; Gong, W. L.; Lutze, W.; Shelnutt, J. A,; Franco, R.; Moira, I. *Chem. Mater.* **2000**, *12*, 1510.

40. Xu, D.; Shi, X; Guo, G.; Gui, L.; Tang, Y. *J. Phys. Chem. B* **2000**, *104*, 5016.

41. Yan, H.; He, R.; Jojnson, J.; Law, M.; Saykally, R. J.; Yang, P. *J. Am. Chem. Soc.* **2003**, *125*, 4728.

42. Vaddiraju, S.; Chandrasekaran, H.; Sunkara, M. K. *J. Am. Chem. Soc.* **2003**, *125*, 10792.

43. Tang, Z.; Kotov, N. A.; Giersig, M. *Science* **2002**, *297*, 237.

44. Barrelet, C. J.; Wu, Y.; Bell, D. C.; Lieber, C. M. *J. Am. Chem. Soc.* **2003**, *125*, 11498.

45. Zhang, D.; Qi, L.; Ma, J. Cheng, H. *Chem. Mater.* **2001**, *13*, 2753.

46. Jiang, X.; Herricks, T.; Xia, Y. *Nano Letters* **2002**, *2*, 1333.

47. Hu, J. Q.; Li, Q.; Meng, X. M.; Lee, C. S.; Lee, S. T. *Chem. Mater.* **2003**, *15*, 305.

48. Zhou, P.; Xue, D.; Lau, H.; Chen, X. *Nano Letters* **2002**, *2*, 845.

49. Yan, H.; Park, S. H.; Finkelstein, G.; Rief, J. H.; LaBean, T. h. *Science* **2003**, *301*, 1885.

50. Liu, Y.; Qian, Y.; Zhang, M.; Chen, Z.; Wang, C. Materials Letters 1996, 26, 81.

51. Qiao, Z. P.; Xie, Y.; Xu, J. G.; Zhu, Y. J.; Qian, Y. T. *Journal of Colloid and Interface Science* **1999**, *214*, 459.

52. Liu, H.; Gu, X.; Xu, X.; Zhang, Z.; Zhang, M. *Radiation Physics and Chemistry* **1999**, *55*, 357.

53. Janata, E. *Radiation Physics and Chemistry* **1996**, *47*, 29.

54. Yin, Y.; Xu, X.; Ge, X.; Lu, Y.; Zhang, Z. *Radiation Physics and Chemistry* **1999**, *55*, 353.

55. Wang, S.; Xin, H. *Radiation Physics and Chemistry* **1999**, *56*, 576.

56. Qiao, Z.; Xie, Y.; Huang, J.; Zhu, Y.; Qian, Y. *Radiation Physics and Chemistry* **2000**, *58*, 287.

57. Mostafavi, M.; Liu, Y.; Pernot, P.; Belloni, J. *Radiation Physics and Chemistry* **2000**, *59*, 49.

58. Seino, S.; Yamamoto, T. A.; Fujimoto, R.; Hashimoto, K.; Katsura, M.; Okuda, S.; Okitsu, K. *Journal of Nuclear Science and Technology* **2001**, *38*, 633.

59. Ni, Y.; Ge, X.; Liu, H.; Xu, X.; Zhang, Z. *Radiation Physics and Chemistry* **2001**, *61*, 61.

60. Ge, X.; Ni, Y.; Zhang, Z. *Radiation Physics and Chemistry* **2002**, *64*, 223.

61. Abe, Y.; Takigami, M.; Sugino, K.; Taguchi, M.; Kojima, T.; Umemura, T.; Tsunoda, K. *Bull. Chem. Soc. Jpn.* **2003**, *76*, 1681.

62. Poole, C. P. Jr.; Owens, F. J. *Introduction to Nanotechnology*; John Wiley & Sons, Inc.: New York, 2003.

63. Klabunde, K. J. *Nanoscale Materials in Chemistry*; John Wiley & Sons, Inc.: New York, 2001.

64. Spinks, J. W. T.; Woods, R. J. *An Introduction to Radiation Chemistry*; 2 ed.; John Wiley & Sons, Inc.: New York, 1976.

65. Malcolme-Lawes, D. J. *Introduction to Radiochemistry*; John Wiley & Sons, Inc.: New York, 1979.

6. Korean Abstract

반도체 물질인 CdS, CdSe, CdTe, 그리고 ZnS는 새로운 합성 방법인 γ 선 조사로 성공적으로 나노입자, 나노로드, 나노와이어로 합성하였다. γ 선을 이용한 합성 방법은 실온과 대기압의 온화한 조건에서 합성되어졌다. 합성에 계면활성제로서 sodium oleate를 사용하였다. 특히, 나노로드와 나노와이어의 경우 용매로서 ethylendiamine과 pyridine을 사용하였다. XRD, EDX, XPS 등으로 분석하여 합성된 나노입자, 나노로드 그리고 나노와이어의 구조적 특성과 성분분석을 확인하였다. 또한, TEM을 이용하여 크기와 모양을 확인할 수 있었다. 광학적 특성은 흡수스펙트럼과 형광스펙트럼으로 분석할 수 있었다.